NASA Technical Paper 3608

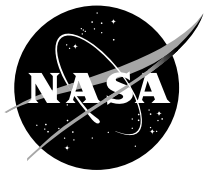

Highly Accurate Beam Torsion Solutions Using the p-Version Finite Element Method

James Smith

March 1996

NASA Technical Paper 3608

Highly Accurate Beam Torsion Solutions Using the p-Version Finite Element Method

James Smith
Lyndon B. Johnson Space Center
Houston, Texas

March 1996

This publication is available from the NASA Center for AeroSpace Information, 800 Elkridge Landing Road, Linthicum Heights, MD 21090-2934, (301) 621-0390.

Contents

Tables

Figures

Because of the font this document was developed in it's difficult to read on-line; it does, however, print cleanly.

Abstract

A new treatment of the classical beam torsion boundary value problem is applied. Using the p-version finite element method with shape functions based on Legendre polynomials, torsion solutions for generic cross-sections comprised of isotropic materials are developed. Element shape functions for quadrilateral and triangular elements are discussed, and numerical examples are provided.

Introduction

There are only a few known exact solutions for the torsion of beams. Among the exact solutions are those for elliptical, rectangular, and triangular cross-sections. The reason so few solutions exist is a problem of elasticity itself; analytical solutions to two- and three-dimensional boundary value problems for irregular areas or volumes are simply difficult to discover. Thus, approximate solutions have to be found. In this context, we extend the highly accurate p-finite element method to the two-dimensional boundary value problem of beam torsion.

Based on Legendre polynomials, the p-finite element method offers exceptional convergence compared to the traditional h-version of the finite element method (Babuska [1]). In the p-version finite element method, the error in the solution is controlled by the polynomial order p, whereas in the h-version, the error is a function of the diameter h of the largest element. The advantages of p-FEM have been exploited in several areas, including elasticity, heat transfer (Smith [5]), and fluid dynamics. This is the first implementation of the method to the torsion problem. Numerical examples will show that its use in torsion problems is indeed valuable. The convergence of the solutions and its derivatives over the range from linear $p = 1$ elements to eighth-order $p = 8$ elements demonstrates the effectiveness of p-FEM to torsion.

Classical Theory of Torsion

In this section, we present the classical theory for torsion of beams for isotropic materials. If we consider a three-dimensional beam of length L with the cross-section shown in Figure 1 in the (x_1, x_2) plane, at the end $x_3 = L$, a torque is applied. At the end $x_3 = 0$, the beam is constrained against rotation (translation of u_1 and u_2 displacements in the plane). Between the ends, the boundary Γ is free of stress.

The state of stress in cross-section domain Ω must satisfy the equations of equilibrium

$$\mathrm{div}\mathbf{T} = 0, \tag{1}$$

where for a linearly elastic, isotropic material, the stress tensor $\mathbf{T}$ is expressed in terms of the Lamé constants λ and μ and the linear strain tensor $\mathbf{E}$ as

$$\mathbf{T} = \lambda\,(\mathrm{tr}\mathbf{E})\,\mathbf{I} + 2\mu\mathbf{E}. \tag{2}$$

The linear strain tensor $\mathbf{E}$ is given by

$$\mathbf{E} = \frac{1}{2}\left[\mathrm{grad}\mathbf{u} + (\mathrm{grad}\mathbf{u})^T\right], \tag{3}$$

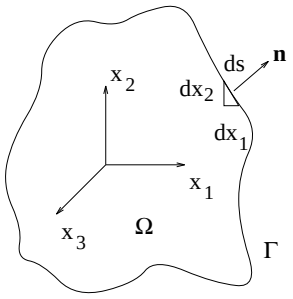

Figure 1. **Torsion problem domain.**

where $\mathbf{u}$ is the displacement vector. In addition, the stresses must satisfy the condition on Γ of

$$\mathbf{Tn} = 0, \tag{4}$$

where $\mathbf{n}$ is the normal to the surface at any point on Γ.

To solve the set of equations above, we assume a solution (Fung [4], p. 164)

$$u_1 = -\alpha x_2 x_3, \qquad u_2 = \alpha x_1 x_3, \qquad \text{and} \qquad u_3 = \alpha\phi(x_1, x_2), \tag{5}$$

where α is the angle of twist per unit length of the beam, and $\phi(x_1, x_2)$ is the warping function. In (5), it is assumed that α is small such that the strains are strictly linear. Inserting (5) into (2), we find that the only nonzero stresses are

$$T_{13} = \mu\alpha\left(\frac{\partial\phi}{\partial x_1} - x_2\right) \qquad \text{and} \qquad T_{23} = \mu\alpha\left(\frac{\partial\phi}{\partial x_2} + x_1\right). \tag{6}$$

It should be noted that equations (6) identically satisfy (1) if we introduce the relations

$$T_{13} = \mu\alpha\frac{\partial\psi}{\partial x_2} \qquad \text{and} \qquad T_{23} = -\mu\alpha\frac{\partial\psi}{\partial x_1}, \tag{7}$$

where $\psi(x_1, x_2)$ is the stress function.

Differentiating the first equation in (6) with respect to x_2 and the second equation in (6) with respect to x_1 and using (7), we have

$$\frac{\partial T_{13}}{\partial x_2} = \mu\alpha\left(\frac{\partial^2\phi}{\partial x_1\partial x_2} - 1\right) = \mu\alpha\frac{\partial^2\psi}{\partial x_2^2} \tag{8}$$

and

$$\frac{\partial T_{23}}{\partial x_1} = \mu\alpha\left(\frac{\partial^2\phi}{\partial x_1\partial x_2} + 1\right) = -\mu\alpha\frac{\partial^2\psi}{\partial x_1^2}. \tag{9}$$

Subtracting equation (9) from (8) yields

$$\frac{\partial^2\psi}{\partial x_1^2} + \frac{\partial^2\psi}{\partial x_2^2} = -2, \tag{10}$$

which is the governing differential equation for the torsion problem for a linearly elastic, isotropic material. Recalling equation (4), we must meet the boundary condition, which is written as

$$T_{31}n_1 + T_{32}n_2 = \mu\alpha\left(\frac{\partial\psi}{\partial x_2}n_1 - \frac{\partial\psi}{\partial x_1}n_2\right) = 0. \tag{11}$$

From Figure 1, we see that

$$n_1 = \frac{dx_2}{ds} \qquad \text{and} \qquad n_2 = -\frac{dx_1}{ds}, \tag{12}$$

such that (11) can be rewritten as

$$\frac{\partial\psi}{\partial s} = 0 \qquad \text{on } \Gamma. \tag{13}$$

Therefore, ψ is constant on the boundary Γ, and we can set $\psi = 0$ on Γ without loss of generality.

The magnitude of the shear stress is given by

$$\tau = \sqrt{T_{13}^2 + T_{23}^2} = \mu\alpha\sqrt{\left(\frac{\partial\psi}{\partial x_1}\right)^2 + \left(\frac{\partial\psi}{\partial x_2}\right)^2} \tag{14}$$

anywhere in the cross-section. In addition, the moment of the external forces at the end of the beam is

$$M = \int_\Omega (x_1T_{23} - x_2T_{13})\,d\Omega = -\mu\alpha\int_\Omega\left(x_1\frac{\partial\psi}{\partial x_1} + x_2\frac{\partial\psi}{\partial x_2}\right)d\Omega = D\alpha, \tag{15}$$

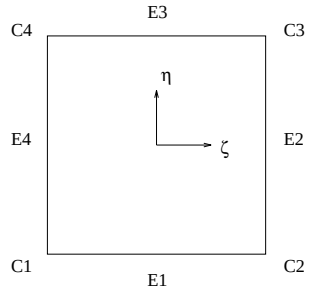

Figure 2. **Standard quadrilateral element geometry.**

where D is the torsional rigidity of the cross-section, or

$$D = -\mu \int_\Omega \left(x_1 \frac{\partial \psi}{\partial x_1} + x_2 \frac{\partial \psi}{\partial x_2} \right) d\Omega = 2\mu \int_\Omega \psi d\Omega, \tag{16}$$

where Green's theorem and $\psi = 0$ on Γ have been used.

In summary, the torsion problem is governed by the equations

$$\nabla^2 \psi = -2 \qquad \text{in } \Omega, \qquad \psi = 0 \qquad \text{on } \Gamma, \tag{17}$$

with the stress magnitude given by (14) and the torsional rigidity by (16).

Finite Element Solution of the Torsion Problem

To solve equation (17), we apply Galerkin's method. This method requires us to write the error residual

$$R = \nabla^2 \psi + 2 \tag{18}$$

and integrate it against a set of trial functions N_i over Ω such that

$$\int_\Omega R N_i d\Omega = \int_\Omega \left(\nabla^2 \psi + 2 \right) N_i d\Omega = 0. \tag{19}$$

The first term in equation (19) can be expanded through integration by parts as

$$\int_\Omega \nabla^2 \psi N_i d\Omega = -\int_\Omega \left(\frac{\partial \psi}{\partial x_1} \frac{\partial N_i}{\partial x_1} + \frac{\partial \psi}{\partial x_2} \frac{\partial N_i}{\partial x_2} \right) d\Omega + \int_\Gamma N_i \frac{\partial \psi}{\partial x_1} n_1 d\Gamma + \int_\Gamma N_i \frac{\partial \psi}{\partial x_2} n_2 d\Gamma, \tag{20}$$

where the boundary terms vanish if (13) is used.

If we write the stress function ψ as

$$\psi = \sum_{j=1}^{N_s} a_j N_j, \tag{21}$$

where a_j are constant coefficients, then (19) can be rewritten as

$$\int_\Omega \left(\frac{\partial N_i}{\partial x_1} \frac{\partial N_j}{\partial x_1} + \frac{\partial N_i}{\partial x_2} \frac{\partial N_j}{\partial x_2} \right) d\Omega a_j = \int_\Omega 2 N_i d\Omega. \tag{22}$$

In terms of a system of equations, we have

$$[K]\{a\} = \{F\}. \tag{23}$$

The parameter N_s is the number of trial shape functions N_j (or N_i) to be used in the solution.

Shape Functions for Quadrilateral Elements

Before actually stating the shape functions used for the two-dimensional quadrilateral element, we should examine the geometry used. Figure 2 shows the quadrilateral element to be examined. The element has 4 corners, 4 edges, and one interior, each of which must have shape functions associated with it. The corners in Figure 2 are labeled C1 to C4, and the coordinates of the corners in a (ζ, η) coordinate system are located at locations $(\pm 1, \pm 1)$. The origin $(\zeta, \eta) = (0, 0)$ is located at the center of the quadrilateral element in the parametric space.

There is one mode associated with each corner for polynomial levels of $p = 1$ and up. These shape functions are given by the functions

$$N_{Ci} = f(\zeta, \eta), \tag{24}$$

where the C in (24) denotes a corner mode, and i refers to the corner number. Explicitly, the corner modes are given by

$$N_{C1} = \frac{1}{4}(1-\zeta)(1-\eta), \tag{25}$$

$$N_{C2} = \frac{1}{4}(1+\zeta)(1-\eta), \tag{26}$$

$$N_{C3} = \frac{1}{4}(1+\zeta)(1+\eta), \tag{27}$$

and

$$N_{C4} = \frac{1}{4}(1-\zeta)(1+\eta). \tag{28}$$

Starting with $p = 2$, edge modes for the quadrilateral element are prescribed. For each additional polynomial level, four modes are added to the total number of degrees of freedom for the element, corresponding to the number of edges on the element. Thus, for any given polynomial order, we have $4(p-1)$ edge modes, defined by

$$N_{Ep}^{(i)}(\zeta, \eta) = f(\zeta, \eta), \tag{29}$$

where E refers to the fact that this is an edge mode, p is the polynomial order of the element, and i is the edge number. These modes are written in terms of integrals of the Legendre polynomials such that

$$N_{Ei}^{(1)} = \frac{1}{2}(1-\eta)\phi_i(\zeta), \tag{30}$$

$$N_{Ei}^{(2)} = \frac{1}{2}(1+\zeta)\phi_i(\eta), \tag{31}$$

$$N_{Ei}^{(3)} = \frac{1}{2}(1+\eta)\phi_i(\zeta), \tag{32}$$

and

$$N_{Ei}^{(4)} = \frac{1}{2}(1-\zeta)\phi_i(\eta), \tag{33}$$

where the functions ϕ_i are defined by

$$\phi_i(\alpha) = \sqrt{\frac{2i-1}{2}} \int_{-1}^{\alpha} P_{i-1}(x)dx, \tag{34}$$

and the functions $P_j(x)$ are the Legendre polynomials of order j.

For polynomial levels of degree $p = 4$ and up, internal modes become evident in the quadrilateral element. The internal modes are restricted to nonzero values inside the element (not at the corners or edges). The internal mode for a p level of 4 is given by

$$N_4^{(0)} = (1-\zeta^2)(1-\eta^2), \qquad p \geq 4 \tag{35}$$

where the the subscript refers to the polynomial level, and the superscript denotes that this is an internal mode.

p	Corner Modes	Edge Modes	Internal Modes	Total DOF
1	4			4
2	4	4		8
3	4	8		12
4	4	12	1	17
5	4	16	3	23
6	4	20	6	30
7	4	24	10	38
8	4	28	15	47

Table 1. **Degree of freedom chart for quadrilateral elements**

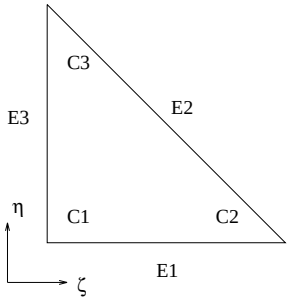

Figure 3. **Standard triangular element geometry.**

For higher modes, we can write the shape functions in terms of the shape functions for $p = 4$. That is, the shape functions for $p = 5$ and up have kernels composed of the shape function (35). For $p = 5$, there are two additional shape functions, given by

$$N^{(0)}_{5,\{1,2\}} = N^{(0)}_4\{P_1(\zeta), P_1(\eta)\}, \qquad p \geq 5 \tag{36}$$

where $P_i(\alpha)$ are Legendre polynomials of order i. The notation used in equation (36) associates two different functions with two different shape functions. For example, in equation (36), we have two shape functions, $N^{(0)}_{5,1}$ and $N^{(0)}_{5,2}$ written as functions of $P_1(\zeta)$ and $P_1(\eta)$, respectively.

For the higher polynomial levels, we can write the face shape functions like

$$N^{(0)}_{6,\{1,2,3\}} = N^{(0)}_4\{P_2(\zeta), P_2(\eta), P_1(\zeta)P_1(\eta)\}, \qquad p \geq 6 \tag{37}$$

$$N^{(0)}_{7,\{1,2,3,4\}} = N^{(0)}_4\{P_3(\zeta), P_3(\eta), P_2(\zeta)P_1(\eta), P_1(\zeta)P_2(\eta)\}, \qquad p \geq 7 \tag{38}$$

and

$$N^{(0)}_{8,\{1,2,3,4,5\}} = N^{(0)}_4\{P_4(\zeta), P_4(\eta), P_3(\zeta)P_1(\eta), P_1(\zeta)P_3(\eta), P_2(\zeta)P_2(\eta)\}. \qquad p \geq 8 \tag{39}$$

Now that the shape functions have been written, we can easily determine the number of equations that will be needed for the analysis. We shall refer to the number of equations associated with a solution variable as the number of degrees of freedom per variable. The number of equations associated with each polynomial order is given in Table 1.

Shape Functions for Triangular Elements

The shape functions for triangular elements are slightly more difficult since the element contains a slanted edge, as shown in Figure 3. The element has 3 corners, 3 edges, and one interior, each of which must have shape functions associated with them. The corners in Figure 3 are labeled C1 to C3, and the

p	Corner Modes	Edge Modes	Internal Modes	Total DOF
1	3			3
2	3	3		6
3	3	6	1	10
4	3	9	3	15
5	3	12	6	21
6	3	15	10	28
7	3	18	15	36
8	3	21	21	45

Table 2. **Degree of freedom chart for triangular elements**

coordinates of the corners in a (ζ, η) coordinate system are located at locations $(0,0)$, $(1,0)$, and $(0,1)$ in the parametric space.

There is one mode associated with each corner for polynomial levels of $p = 1$ and up, given by

$$N_{C1} = 1 - \zeta - \eta, \tag{40}$$

$$N_{C2} = \zeta, \tag{41}$$

and

$$N_{C3} = \eta. \tag{42}$$

Starting with $p = 2$, three edge modes are added to the total number of degrees of freedom for the element. Thus, for any given polynomial order, we have $3(p-1)$ edge modes, defined by

$$N_{Ei}^{(1)} = (1 - \zeta - \eta)\phi_i(\zeta), \tag{43}$$

$$N_{Ei}^{(2)} = \eta\phi_i(\zeta), \tag{44}$$

and

$$N_{Ei}^{(3)} = (1 - \zeta - \eta)\phi_i(\eta). \tag{45}$$

For polynomial levels of degree $p = 3$ and up, internal modes become evident in the triangular element. The internal mode for a p level of 3 is given by

$$N_3^{(0)} = L_1 L_2 L_3, \qquad p \geq 3 \tag{46}$$

where the functions L_1, L_2, and L_3 are defined as

$$L_1 = 1 - \zeta - \eta, \qquad L_2 = \zeta, \qquad \text{and} \qquad L_3 = \eta. \tag{47}$$

For higher modes, we can write the shape functions in terms of the shape functions for $p = 3$. That is, the shape functions for $p = 4$ and up have kernels composed of the shape functions (46). For $p = 4$, there are two additional shape functions, given by

$$N_{4,\{1,2\}}^{(0)} = N_3^{(0)}\{P_1(L_2 - L_1), P_1(2L_3 - 1)\}. \qquad p \geq 4 \tag{48}$$

The remaining internal modes are given by

$$N_{5,\{1,2,3\}}^{(0)} = N_3^{(0)}\{P_2(L_2 - L_1), P_2(2L_3 - 1), P_1(L_2 - L_1)P_1(2L_3 - 1)\}, \qquad p \geq 5 \tag{49}$$

$$N_{6,\{1,2,3,4\}}^{(0)} = N_3^{(0)}\{P_3(L_2 - L_1), P_3(2L_3 - 1), P_2(L_2 - L_1)P_1(2L_3 - 1), P_1(L_2 - L_1)P_2(2L_3 - 1)\}, \qquad p \geq 6 \tag{50}$$

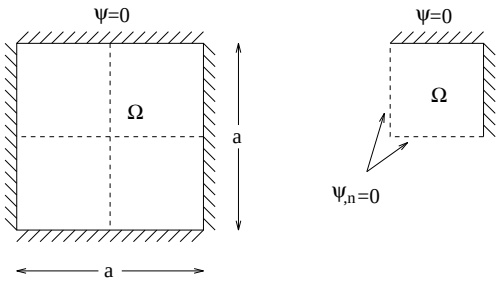

Figure 4. **Single-element meshes for full and quarter models.**

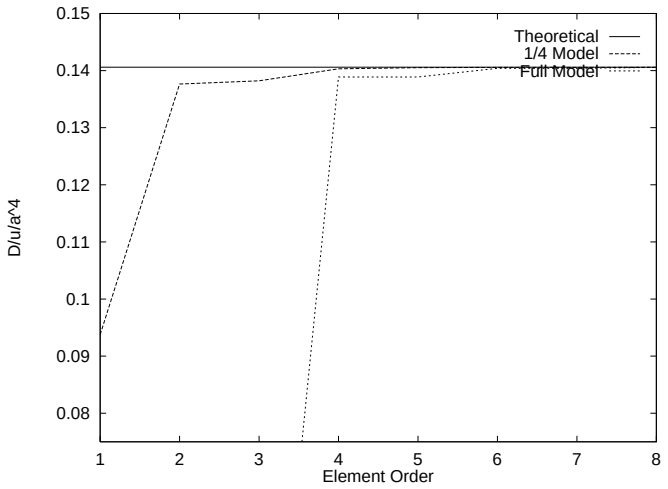

Figure 5. **Dimensionless torsional constant versus p-level for a square beam.**

$$N^{(0)}_{7,\{1,2,3,4,5\}} = N^{(0)}_3\{P_4(L_2-L_1), P_4(2L_3-1), P_3(L_2-L_1)P_1(2L_3-1), P_1(L_2-L_1)P_3(2L_3-1), P_2(L_2-L_1)P_2(2L_3-1)\}, \qquad p \geq 7 \quad (51)$$

and

$$N^{(0)}_{8,\{1,2,3,4,5,6\}} = N^{(0)}_3\{P_5(L_2-L_1), P_5(2L_3-1), P_4(L_2-L_1)P_1(2L_3-1), P_1(L_2-L_1)P_4(2L_3-1), P_3(L_2-L_1)P_2(2L_3-1), P_2(L_2-L_1)P_3(2L_3-1)\}. \qquad p \geq 8 \quad (52)$$

The number of equations associated with each polynomial order for triangular elements is given in Table 2. As can be seen from Table 2, there is not much difference between the total number of degrees of freedom associated with a triangular element and that of the quadrilateral element, shown in Table 1. Thus, it is preferable to use quadrilateral elements when defining geometry.

Torsion of Beams with Square Cross-Sections

In this section, we demonstrate the use of the p-version finite element method for torsion problems. If we consider a beam with a square cross-section, then we can write the exact solutions for the maximum torsional shear stress and torsional constant as (Sokolnikoff [6], p. 131-132)

$$\tau_{max} = \mu\alpha a\left\{1 - \frac{8}{\pi^2}\left[\frac{1}{\cosh\pi/2} + \sum_{n=1}^{\infty}\frac{1}{(2n+1)^2\cosh(2n+1)\pi/2}\right]\right\} \quad (53)$$

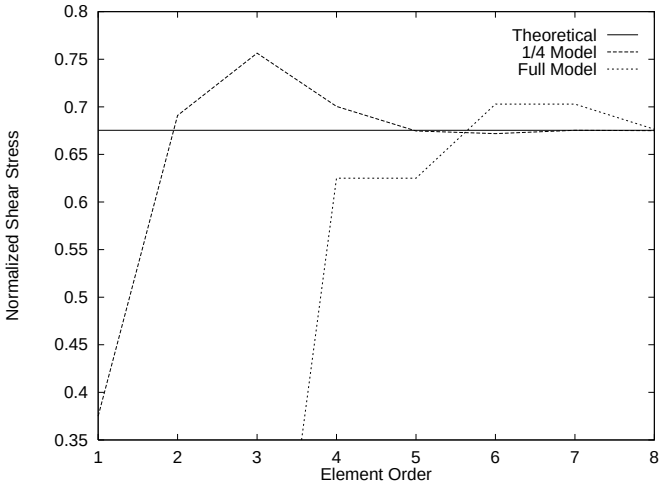

Figure 6. **Dimensionless torsional shear stress versus p-level for a square beam.**

and

$$D = \mu a^4 \left[\frac{1}{3} - \frac{64}{\pi^5} \sum_{n=0}^{\infty} \frac{\tanh(2n+1)\pi/2}{(2n+1)^5} \right], \tag{54}$$

where a is the length of one of the sides of the cross-section, μ is the shear modulus of the beam material, and α is the angle of twist per unit length of the beam.

To compare the analytical solutions (53) and (54) to the finite element solutions, we consider two different meshes. First, if we consider the left mesh of Figure 4, we have a single element representing the domain Ω. Next, by exploiting the double symmetry of the cross-section, we can model one-quarter of the cross-section, yielding the second mesh in Figure 4. We note that in this mesh, on two sides we have $\partial\psi/\partial n = 0$.

In Figure 5 we show the convergence of the normalized torsional constant $D/\mu a^4$ as the polynomial order of the solution is increased. The flat, horizontal line is the value given by equation (54). It should be noted that for the full model, there are no computed values of the normalized torsional constant until $p = 4$. The reason for this is that from $p = 1$ to $p = 3$, there are only corner and edge modes. Since $\psi = 0$ on the boundary, then clearly the solution contains no active degrees of freedom, and the solution is forced to zero. However, at $p = 4$, we obtain the first internal mode, and its value is reflected in the computation of a non-zero torsional constant. At $p = 4$, the full model mesh only has the single active degree of freedom, yet its computed torsional constant value has less error than the quarter model for $p = 3$, which has more degrees of freedom. Thus, it appears that additional degrees of freedom are not terribly important in evaluating function values.

However, when shear stresses, which are derivatives of the trial solution, are evaluated, the calculated flux values are somewhat dependent upon the order of the solution, as seen in Figure 6. Again, for $p = 1$ to $p = 3$, the one-element full model solution is identically zero since all of the degrees of freedom are constrained to zero from the $\psi = 0$ restriction. Thus, the derivatives are also zero. However, with increasing p, we do see the existence of a derivative value for the full model, and over the entire p range, the quarter-model shows exceptional convergence.

Torsion of an Elliptically Shaped Beam

The simple cross-section of the previous section can be expanded to a beam with an elliptical cross-section. The ellipse provides yet another known theoretical solution against which the numerical finite element solution can be compared. In this case, the maximum shear stress due to torsion, which occurs closest to

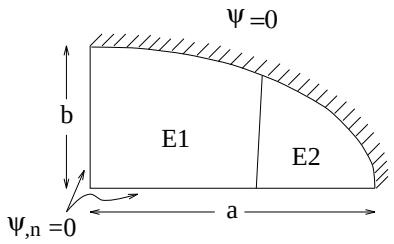

Figure 7. **Two element mesh for quarter-model of elliptical section.**

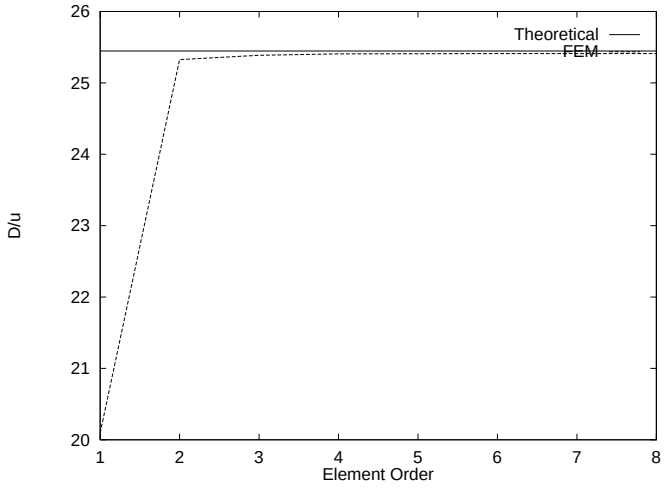

Figure 8. **Dimensionless torsional constant versus p-level for an elliptical beam.**

the major and minor axes of the ellipse, and the torsional rigidity are given by (Fung [4], p. 170)

$$\tau_{max} = 2\mu\alpha \frac{a^2 b}{a^2 + b^2} \tag{55}$$

and

$$D = \mu \frac{\pi a^3 b^3}{a^2 + b^2}, \tag{56}$$

where a and b are the major and minor axes of the ellipse.

For the comparison, a simple two-element mesh representing one-quarter of the entire ellipse is employed. One quadrilateral element and one triangular element are used, as shown in Figure 7. For an ellipse with $a = 3$ and $b = 1.5$, we find that for $p \geq 2$, there is good agreement with the normalized torsional rigidity D/μ, as shown in Figure 8. Likewise, there is rapid convergence of the normalized shear stress τ_{max}/μ, as shown in Figure 9. The reason for the quick convergence is that the exact solution is given by (Fung [4], p. 169)

$$\psi = -\mu\alpha \frac{a^2 b^2}{a^2 + b^2} \left(\frac{x^2}{a^2} + \frac{y^2}{b^2} - 1 \right). \tag{57}$$

Since (57) is quadratic in x and y, the theoretical solution is quickly converged for $p = 2$, which is shown in the graphs for the torsional constant and the maximum shear stress.

Torsion of a Generic Section with Cutouts

Textbook solutions for the torsion problem can be demonstrated with finite element methods easily, but they are fairly uninteresting and show only that we can match solutions. To demonstrate the effectiveness

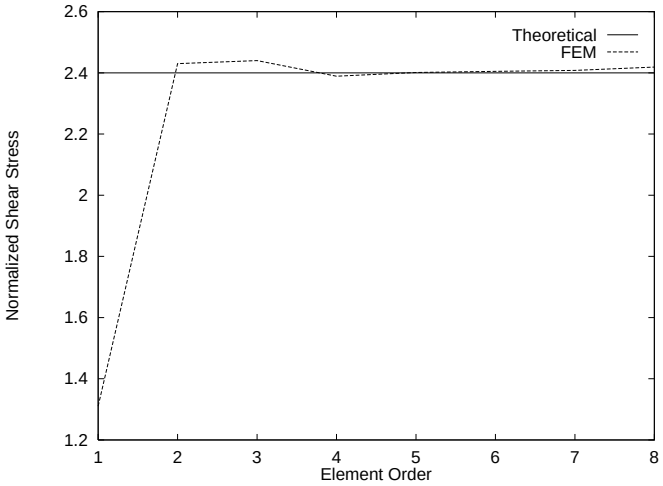

Figure 9. **Dimensionless torsional shear stress versus p-level for an elliptical beam.**

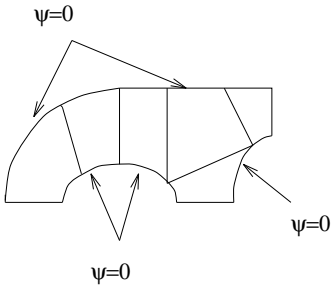

Figure 10. **Finite element mesh of a generic cross-section.**

of the finite element method to torsion, especially with p-finite elements, we examine the torsion of the cross-section shown in Figure 10. The cross-section has symmetry about two axes, so only one-quarter of the cross-section is modeled. Along the outside of the section, the function ψ is identically zero. Likewise, along the perimeter of the cutouts, the stress function is forced to zero. Along the straight edges, which represent lines of symmetry, we have the condition $\partial\psi/\partial n = 0$. The finite element mesh is a seven-element mesh using eight noded elements to achieve the curvature along the edges.

The cross-section is excellent at demonstrating the torsion of multiply connected regions which would otherwise be left unsolved by analytical means. The torsion analysis was conducted with element shape functions from $p = 2$ to $p = 8$. The results for $p = 1$ are inconclusive since the $p = 1$ shape functions are corner modes, and the mesh requires that $\psi = 0$ at the corners. The convergence of the torsional constant is shown in Figure 11, whereas the shear stress at a point in the left cutout is shown in Figure 12. Like the cases shown previously, we find rapid convergence for both the function value and the first derivative.

Finally, an error estimate of the solution is plotted in Figure 13. Two separate mesh strategies were employed in this analysis. The first mesh is the same as shown in Figure 10. That is, the mesh remains the same, but the polynomial order of the solution is increased from $p = 2$ to $p = 8$. The second mesh strategy is to take the mesh of Figure 10 and subdivide the areas into smaller regions with uniform h-refinement. That is, each element is subdivided into n^2 elements, where n is the number of elements per side. This yields a uniform h-refinement and comparison curve to demonstrate the convergence of the new technique. The error in the mesh is plotted in Figure 13 versus the number of active degrees of freedom in the solution, and it is defined as

$$\epsilon = |D_{mesh} - D_{\infty}|, \tag{58}$$

where D_{mesh} is the torsional constant corresponding to the current mesh and D_{∞} is the torsional constant

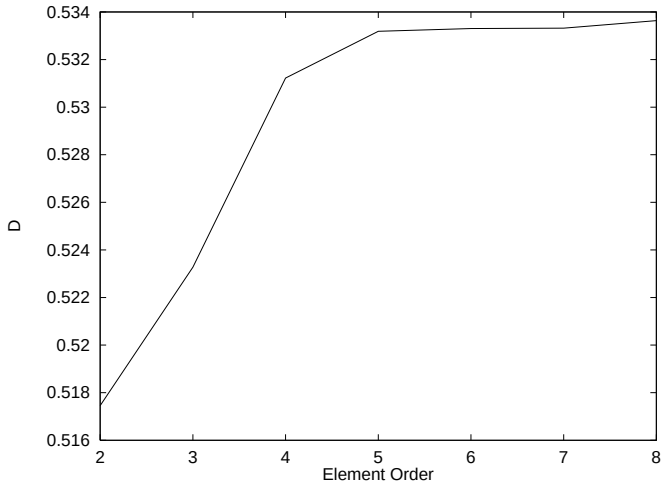

Figure 11. **Torsional constant versus p-level of the solution.**

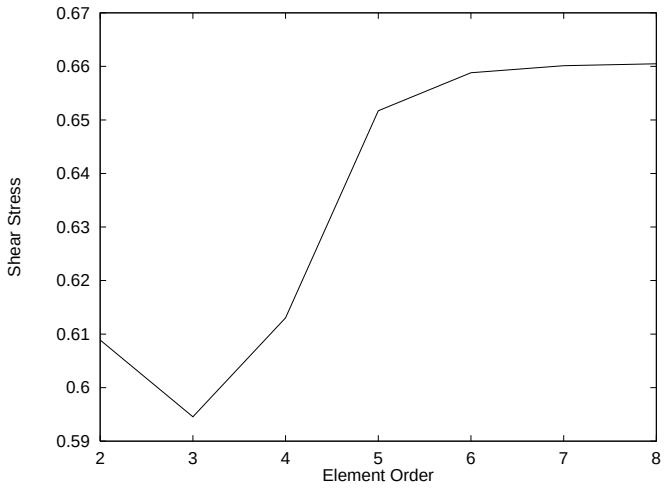

Figure 12. **Torsional shear stress versus p-level of the solution.**

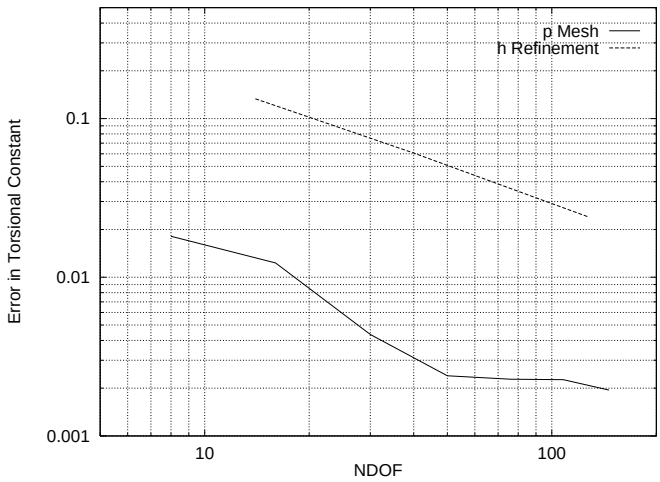

Figure 13. **Error estimates for the p-element and refined h-element meshes.**

computed for a mesh with $p = 8$ and a significant number of elements. In Figure 13, we note the exceptional performance of the p-version mesh. While the refined h mesh converges at virtually a constant rate, the p-element mesh, composed of just 6 elements, rapidly converges with the addition of higher order polynomials.

Conclusions

As demonstrated by the examples, implementing the p-version of the finite element method is beneficial in achieving highly accurate, converged solutions to the torsion boundary value problem. The flexibility of increasing the fidelity of the solution by changing the polynomial order rather then remeshing to find appropriate element size saves both time and effort without sacrificing numerical accuracy. Indeed, it was shown that for equal degrees of freedom, the p-method far outperforms the h-method in the calculation of the torsional constant. While no results for the shear stresses were presented with the general cross-section, we would expect similar if not better characteristics, as the h-method is limited to at best first derivatives which vary linearly in the element space. However, for the p-method, the derivatives are of higher order, giving them the ability to match gradients better.

References

[1] Babuska, I., "The $h-p$ version of the finite element method for problems with nonhomogeneous essential boundary conditions," *Computer Methods Appl. Mech. Engrg.*, (74), 1-28, 1989.

[2] Boas, M.L., *Mathematical Methods in the Physical Sciences*, John Wiley and Sons, New York, 1983.

[3] Burnett, D.S., *Finite Element Analysis*, Addison-Wesley, Reading, Massachusetts, 1987.

[4] Fung, Y.C., *Foundations of Solid Mechanics*, Prentice-Hall, Englewood Cliffs, New Jersey, 1965.

[5] Smith, J., and Madden, C., "The p-Finite Element Method Applied to Transient Thermoelastic Problems," presented at the 36th AIAA SDM Conference, April 1995, New Orleans, Louisiana, AIAA 95-1269.

[6] Sokolnikoff, I.S., *Mathematical Theory of Elasticity*, McGraw-Hill, New York, 1956.